Electronic Supplementary Information (ESI)

Al-modified Ti-MOR as a robust catalyst for cyclohexanone ammoximation with enhanced anti-corrosion performance

Rusi Peng,[a] Zhipeng Wan,[a] Huanzhi lv,[b] Yejun Guan,[a] Hao Xu*[a] and Peng Wu*[a]

[a] Shanghai Key Laboratory of Green Chemistry and Chemical Processes, School of Chemistry and Molecular Engineering, East China Normal University, North Zhongshan Road 3663, Shanghai, 200062, P.R. China

[b] Zhejiang JRT New Material Co. Ltd, Fuling Rd. 1567, Nanming Street, Liandu District, Lishui, 323000, Zhejiang Province, China

Corresponding authors: pwu@chem.ecnu.edu.cn (P. WU); hxu@chem.ecnu.edu.cn (H. XU)

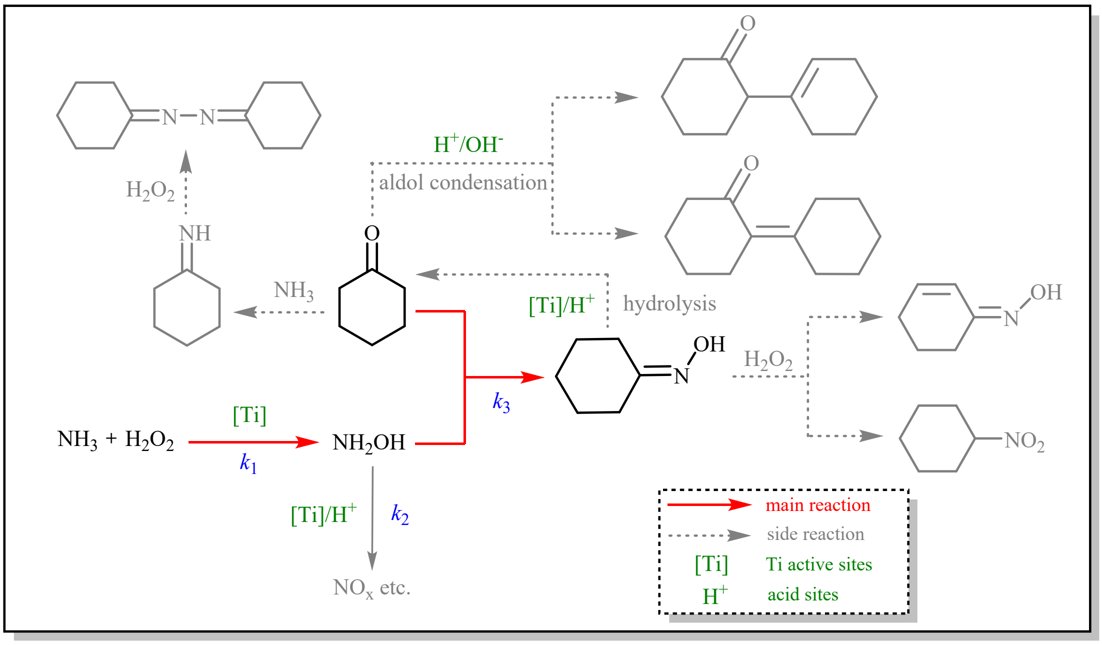

Scheme S1 Reaction network of cyclohexanone ammoximation over titanosilicates.

According to the hydroxylamine route, the side reactions were complicated in the cyclohexanone ammoximation, including but not limited to the condensation and consecutive oxidation of ketone, together with deep oxidation of oximes and decomposition of hydroxylamine. The formation and decomposition of hydroxylamine stayed competitive and affected the apparent activity. However, the rate constant of non-catalytic oximation of cyclohexanone with the hydroxylamine was unaffected by type of titanosilicates.

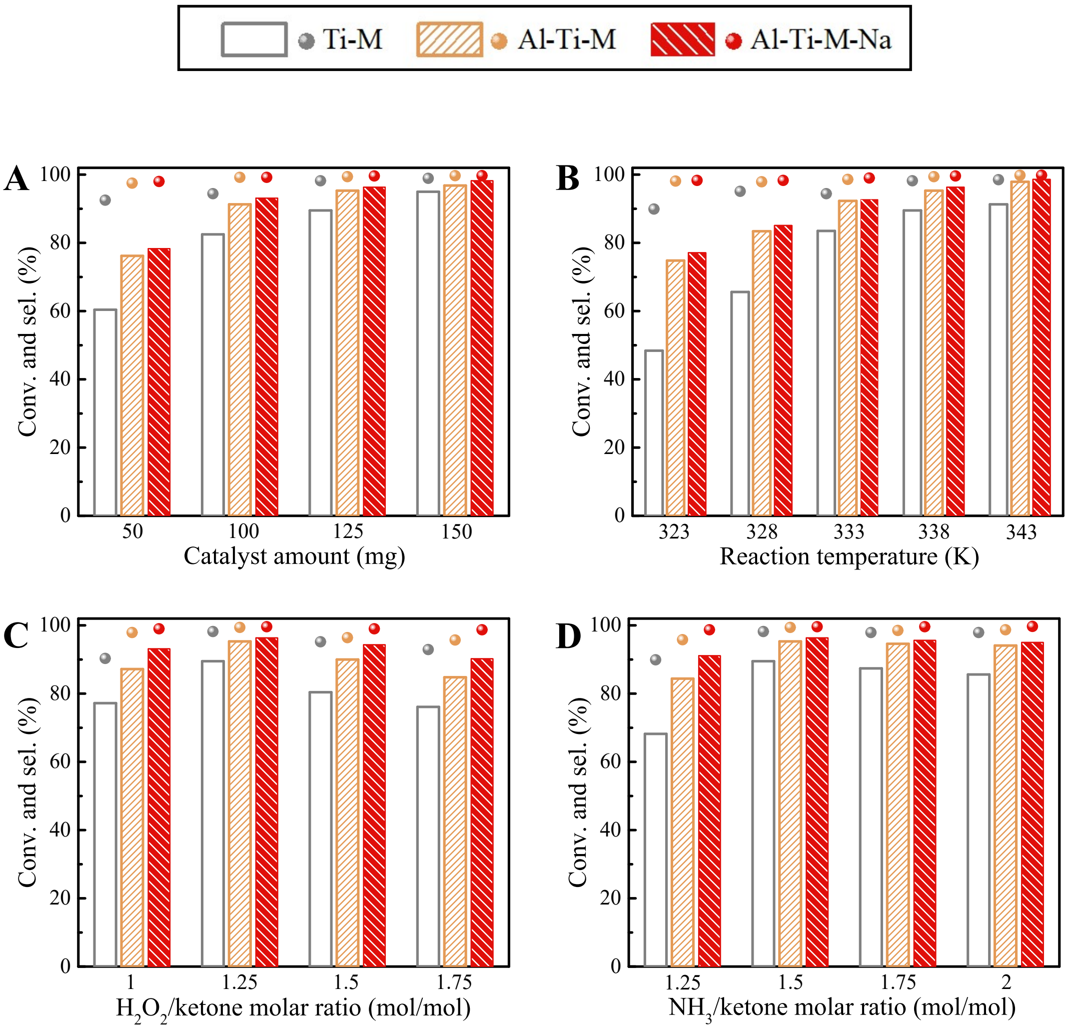

Fig. S1 Effect of catalyst amount (A), reaction temperature (B), H_2O_2/ketone ratio (C) and NH_3/ketone ratio (D) on ketone conversion (bars) and oxime selectivity (balls) in cyclohexanone ammoximation. Reaction conditions: cat., 125 mg (B, C, D); H_2O, 12 g; cyclohexanone, 20 mmol; ketone : H_2O_2 = 1 : 1.25 (A, B, D); ketone : NH_3 = 1 : 1.5 (A, B, C); temp., 338 K (A, C, D); time, 2 h.

For all the three catalysts, the cyclohexanone conversion increased gradually by increasing the catalyst amount and reaction temperature, and then leveled off (Fig.

S1, A and B). Furthermore, a volcano-shaped change was observed over all catalysts with increasing H_2O_2/ketone ratio (Fig. S1C). The ketone conversion and oxime selectivity reached the maximum at a H_2O_2/ketone ratio of 1.25. However, the ketone conversion was significantly decreased along with further increasing H_2O_2 content. With the increase of NH_3/ketone ratio, the cyclohexanone conversion reached a plateau at about 1.5 and remained almost unchanged with a further increase to 2 (Fig. S1D).

Table S1 Element analysis results of fresh and used Ti-M samples.

Sample[a]	Compositions[b]		
	Si/Al	Si/Ti	Si/Na
Ti-M	155	58	/
Ti-M-U	151	57	/
Al-Ti-M	71	57	/
Al-Ti-M-U	72	56	/
Al-Ti-M-Na	75	55	113
Al-Ti-M-Na-U	74	54	239

[a] The samples with suffix “-U” were after five cycles of use in batchwise cyclohexanone ammoximation. Reaction conditions, see Fig. 2.

[b] Molar ratio given by ICP.

After five cycles of use in batchwise cyclohexanone ammoximation, no obvious change over the Si/Al and Si/Ti ratios was observed. However, the Si/Na ratio of used Al-Ti-M-Na increased to 239, indicating the leaching of Na^+ in multiple cycles of reaction.

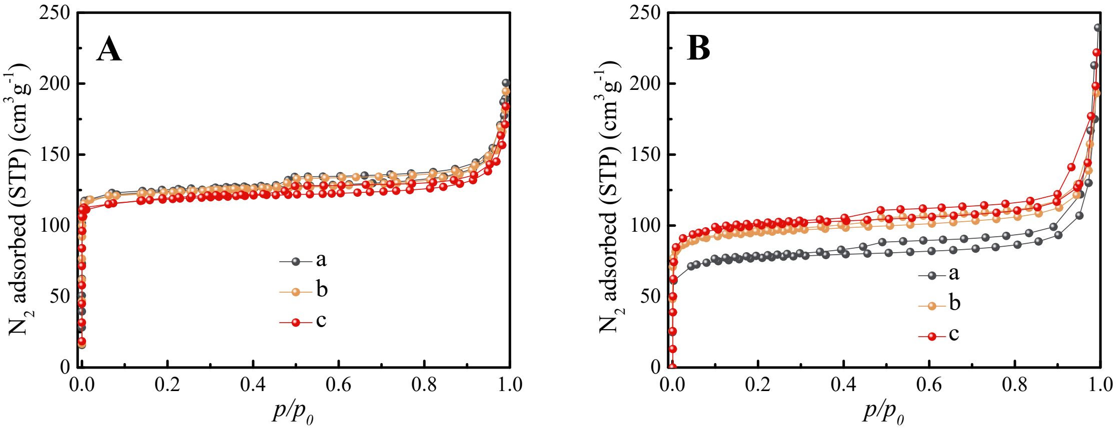

Fig. S2 N_2 adsorption and desorption isotherms of Ti-M (a), Al-Ti-M (b) and Al-Ti-M-Na (c) before (A) and after (B) the treatment with ammonia aqueous solution at 393 K for 12 h.

The aluminated samples both showed similar isotherms as Ti-M, indicating the pores were not blocked by the introduction of Al species and sodium ions. However, after alkaline treatment, the samples all showed an obviously lower N_2 adsorption capacity in the micropore range ($0 < p/p_0 < 0.04$) in comparison to the untreated ones, due to the structure damage by desilication. However, the two aluminated samples showed the sorption capacity in micropore range exceeding that of Ti-M after ammonia treatment. The degradation degree of microporous structure depended on the different anti-corrosion properties of various samples. Obviously, Al-Ti-M and Al-Ti-M-Na are more anti-corrosive than Ti-MOR.

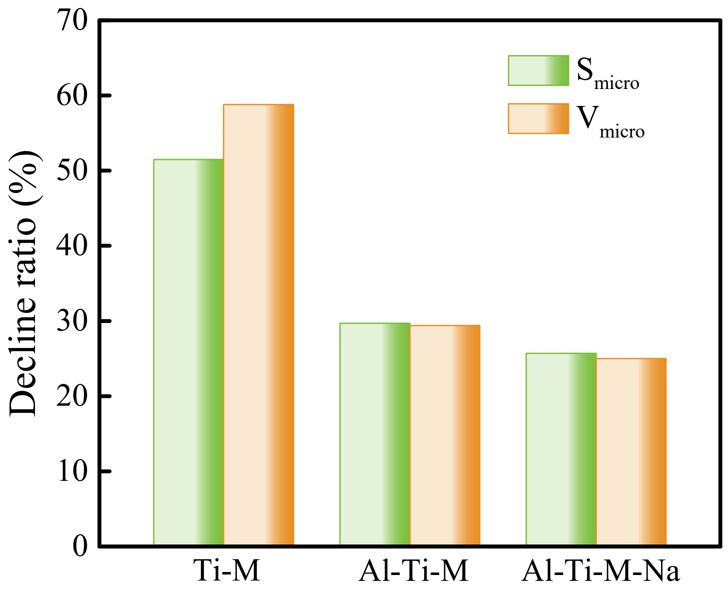

Fig. S3 The decline ratio of microporous characteristics after simulated corrosion process. Alkali treatment condition: 0.2 g zeolite, 3 wt.% NH_3 aqueous solution, liquid: solid = 83.5 : 1 (mass ratio), 393 K, 12 h.

Compared to those of Ti-M-AT, the decline ratio of specific surface areas and micropore volumes over Al-Ti-M-AT and Al-Ti-M-Na-AT were depressed, indicating that more microporous structure was retained during the simulated desilication process.

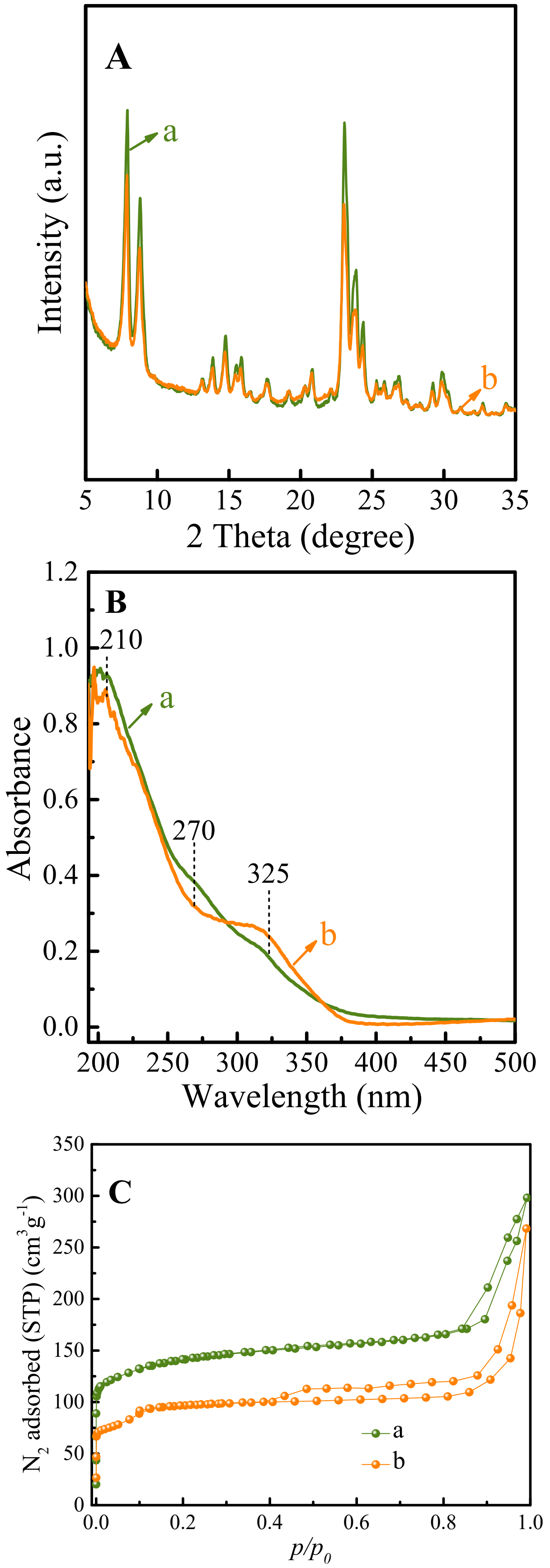
A
a
b
Intensity (a.u.)
5
10
15
20
25
30
35
2 Theta (degree)
B
210
270
325
a
b
Absorbance
0.0
0.2
0.4
0.6
0.8
1.0
1.2
200
250
300
350
400
450
500
Wavelength (nm)
C
a
b
N$_2$ adsorbed (STP) (cm^{3}g^{-1})
0
50
100
150
200
250
300
350
0.0
0.2
0.4
0.6
0.8
1.0
p/p_0

Fig. S4 XRD patterns (A), UV-vis spectra (B) and N_2 adsorption and desorption isotherms of TS-1 before (a) and after (b) alkali treatment. Alkali treatment condition, see Fig. S3.

Compared with TS-1, the treated sample showed a lower crystallinity in XRD pattern and a lower N_2 *adsorption amount in the micropore range* ($0 < p/p_0 < 0.04$)*, indicating the damage of skeleton to a certain degree after alkaline treatment. Besides, the band of anatase phase at 325 nm over TS-1-AT in UV-Vis spectra meant that part of Ti sites were converted to non-catalytic species along with the desilication.*

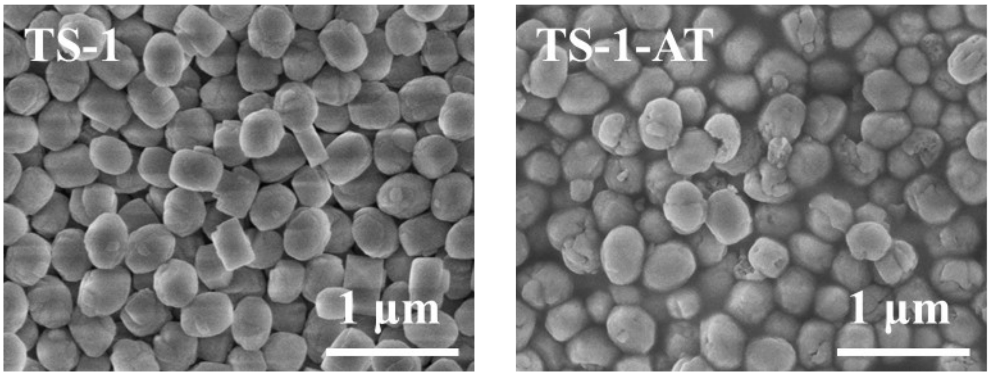

Fig. S5 SEM images of TS-1 and TS-1-AT. Alkali treatment condition, see Fig. S3.

After alkaline treatment, the crystals of TS-1 were broken into smaller crystals with grooves on the surface.

Table S2 Physicochemical properties of TS-1 before and after alkali treatment.

Sample	Si/Ti [a]	SSA ($cm^2\ g^{-1}$)			Pore volume ($cm^3\ g^{-1}$)		
		S_{total} [b]	S_{micro}	S_{ext} [c]	V_{total} [b]	V_{micro} [d]	V_{meso} [c]
TS-1	59	465	388	77	0.39	0.15	0.24
TS-1-AT	55	342	213	129	0.41	0.08	0.33

[a] Molar ratio given by ICP.

[b] Calculated by BET method.

[c] Calculated by *t*-plot method.

[d] $V_{meso} = V_{total} - V_{micro}$.

After simulated basic corrosion, TS-1-AT showed a slightly lower Si/Ti ratio, which indicated the asymmetrical loss of Si and Ti. Meanwhile, the specific surface area and micropore volume decreased obviously over TS-1-AT, indicating the damage of microporous structure during the alkaline treatment.

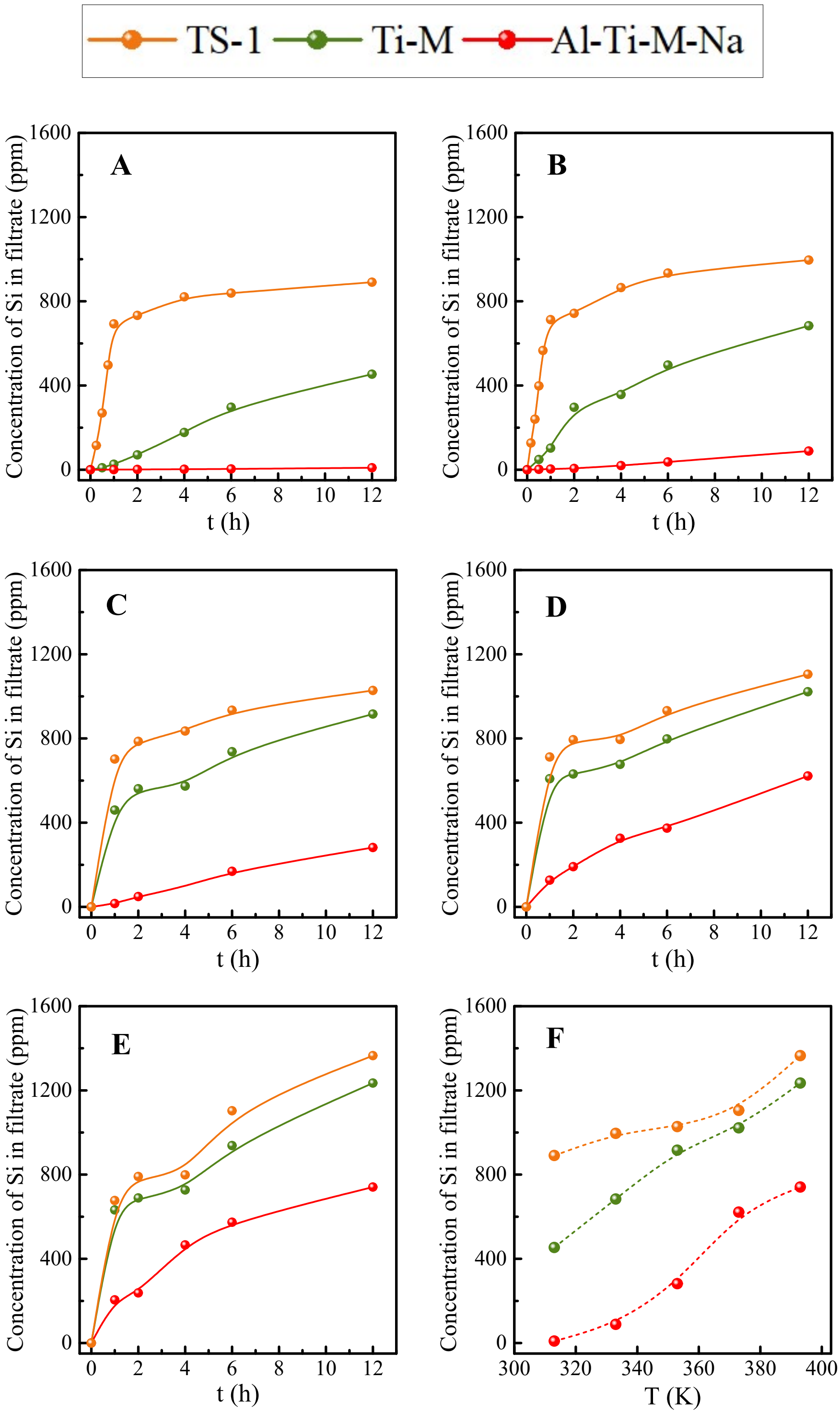

Fig. S6 The dependence of dissolved silicon concentration on the treatment time at 313 K (A), 333 K (B), 353 K (C), 373 K (D), 393 K (E), and that on the treatment temperature (F) of ammonia aqueous solution for 12 h over various titanosilicates.

The concentration of dissolved silicon over various titanosilicates increased with the increase of temperature and treatment time. Compared with the pristine Ti-M, Al-Ti-M-Na showed negligible silicon concentration below 353 K, meaning the aluminated treatment contributed to the enhanced anti-desilication property.

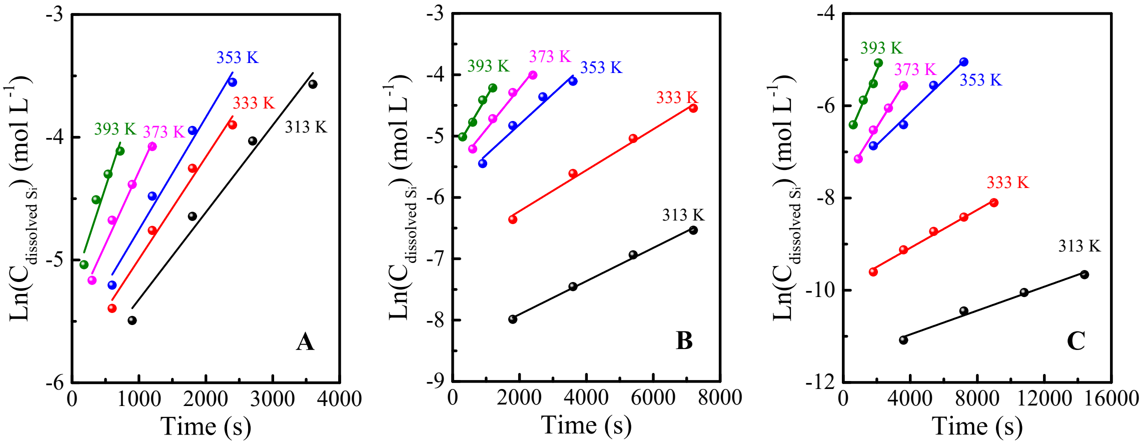

Fig. S7 Kinetics of silicon dissolution of TS-1 (A), Ti-M (B) and Al-Ti-M-Na (C) in 3 wt.% ammonia aqueous solution.

The dissolution rate constant (k) were determined by the ln($C_{Dissolved\ Si}$) versus reaction time at 313, 333, 353, 373 and 393 K. The k values at various temperatures on different titanosilicates were entirely distinct, reflecting the discrepant performances of anti-corrosion over varied samples.

Table S3 The rate constants of the two reaction steps involved in cyclohexanone ammoximation. [a]

Catalyst	Reaction rate constant (mmol L^{-1} min^{-1})	
	k_1 [b]	k_2 [c]
Ti-M	17.5	33.7
Al-Ti-M	25.8	41.2
Al-Ti-M-Na	31.3	29.4

[a] Reaction conditions, see Fig. 12

[b] Hydroxylamine formation

[c] Hydroxylamine decomposition

As for the pristine Ti-M, the hydroxylamine formation rate constant (k_1) and decomposition rate constant (k_2) were 17.5 mmol L^{-1} min^{-1} and 33.7 mmol L^{-1} min^{-1}, respectively. After alumination, Al-Ti-M showed both increased values of k_1 and k_2. However, the Na^+-exchange process endowed Al-Ti-M-Na with a further increase of k_1 value while a decreased value of k_2. This phenomenon indicated that the changes in skeleton and acid sites affected the reaction process.